PCCP

Cavity Transport Effects in Generator-Collector Electrochemical Analysis of Nitrobenzene

Journal:	*Physical Chemistry Chemical Physics*
Manuscript ID:	CP-ART-07-2014-002943.R1
Article Type:	Paper
Date Submitted by the Author:	23-Jul-2014

Complete List of Authors:	Lewis, Grace; University of Bath, Chemistry Dale, Sara; University of Bath, Chemistry Kasprzyk-Hordern, B; University of Bath, Lubben, Anneke; University of Bath, Department of Chemistry Barnes, Edward; University of Oxford, Chemistry Compton, Richard; Oxford University, Department of Chemistry Marken, Frank; Bath University, Department of Chemistry

REVISION

23rd July 2014

Cavity Transport Effects in Generator-Collector Electrochemical Analysis of Nitrobenzene

Grace E. M. Lewis [a], Sara E. C. Dale [a], Barbara Kasprzyk-Hordern [a], Anneke T. Lubben [a], Edward O. Barnes [b], Richard G. Compton [b], and Frank Marken [a]*

[a] *Department of Chemistry, University of Bath, Claverton Down, Bath BA2 7AY, UK*

[b] *Department of Chemistry, Physical and Theoretical Chemistry Laboratory, Oxford University, South Parks Road, Oxford OX1 3QZ, UK*

To be submitted to Physical Chemistry – Chemical Physics

Proofs to F. Marken

Email F.Marken@bath.ac.uk

Abstract

Two types of generator-collector electrode systems, (i) a gold-gold interdigitated microband array and (ii) a gold-gold dual-plate microtrench, are compared for nitrobenzene electroanalysis in aerated aqueous 0.1 M NaOH. The complexity of the nitrobenzene reduction in conjunction with the presence of ambient levels of oxygen in the analysis solution provide a challenging problem in which feedback-amplified generator-collector steady state currents provide the analytical signal. In contrast to the more openly accessible geometry of the interdigitated array electrode, where the voltammetric response for nitrobenzene is less well-defined and signals drift, the voltammetric response for the cavity-like microtrench electrode is stable and readily detectable at 1 μM level. Both types of electrode show oxygen-enhanced low concentration collector current responses due to additional feedback via reaction intermediates. The observations are rationalised in terms of a "cavity transport coefficient" which is beneficial in the dual-plate microtrench, where oxygen interference effects are suppressed and the analytical signal is amplified and stabilised.

Keywords: voltammetry, diffusion, collector-generator, amplification, nitroaromatics, nano-gap sensor.

1. Introduction

Generator – collector electrode systems [1] can offer attractive solutions to a diverse range of electroanalytical problems such as measuring anti-oxidant capacity [2], dopamine detection [3,4], and selective drug detection [5]. Types of electrodes for these measurements vary from ring-disc electrodes [6], dual-hemisphere [7], scanning probe electrodes [8], to channel electrodes [9,10], vibrating electrodes [11] and lithographically manufactured multi-band [12] systems. Most of these electrodes are "openly accessible" (with or without convection) in the sense of offering semi-infinite planar diffusion access for all solution components to the sensor surface. It is interesting to contrast these openly accessible systems to generator-collector electrode systems where a "cavity" allows fast inter-electrode diffusional transport with only limited access to the open solution.

Interest in new electrode geometries has developed in particular with the availability of new lithography-based fabrication methods [13] and better understanding based on new powerful simulation tools [14]. One of the more recent types of generator-collector electrodes is based on the dual-plate microtrench geometry [15] where the feedback current is "internal" with access to the external sample solution via a micro-slit (with micro-band-like diffusion). This geometry may be considered as a "cavity" case (see Figure 1F) and it is of interest to systematically explore "cavity transport effects" where the relative transport rates of bulk solution components and redox cycle components are different.

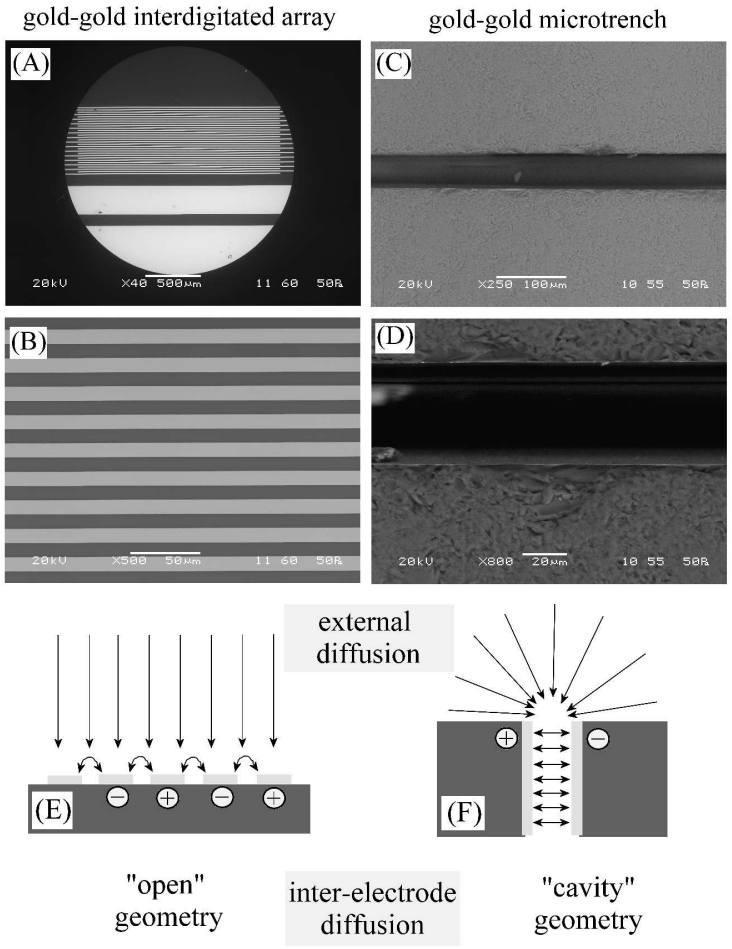

Figure 1. (A,B) SEM images of a gold-gold interdigitated array electrode (Micrux ED-IDA1-Au) with two sets of 15 bands (interdigitated) of length 1.8 mm, width 10 μm, separation 10 μm, and thickness 150 nm. (C,D) SEM images of a gold-gold dual-plate microtrench electrode with 5 mm length, 45 μm width, 300 μm depth (see text), and 100 nm gold film thickness. (E,F) Schematic drawing of "open" and "cavity" generator-collector electrode systems.

In order to evaluate and compare the cases of "open" and "cavity" generator-collector electrode systems, here an interdigitated band array (gold bands 10 μm wide, 10 μm separation, Figure 1A,B) is studied and contrasted to a gold-gold dual-plate electrode (microtrench with 5 mm length, 300 μm depth, 45 μm width, Figure 1C,D). Some recent studies employing dual-plate microtrench electrode systems have addressed the detection of thiols in gold-gold electrodes [16], the detection of protons in platinum-

platinum electrodes [17], and the detection of chloride in dual-boron-doped diamond electrodes [18]. Particularly interesting was the effect of suppressed oxygen signal (observed at dual-tin-doped indium oxide electrodes [19]) due to the irreversible removal of O_2 diffusing into the "mouth" of the dual-plate electrode. A similar effect is investigated here for the reduction of nitrobenzene.

Nitrobenzene may be regarded as a model system for nitro-aromatic analytes [20] many of which are in the class of explosives [21]. The reduction of nitrobenzene follows a complex multi-step mechanism, but when investigated in alkaline solution a distinct "redox-cyclable" one-electron reduction is observed [22]. In this report a comparison of analytical performance is attempted for (i) a gold-gold interdigitated array electrode and (ii) a gold-gold dual-plate microtrench electrode, both with dimensions to give similar steady state generator-collector current responses. Although similar performance is anticipated due to diffusional increase in the detector current, there are secondary issues that strongly affect the detection of nitrobenzene (used here as model analyte) in aqueous 0.1 M NaOH solution (to partially stabilise the nitrobenzene radical anion [23]) and the microtrench electrode appears to be much better suited for this type of analytical problem. Details and effects are complex due to adsorption phenomena at the generator, but collector processes are generally linked to the diffusional access ("open" or "cavity") of analyte and oxygen to the generator-collector electrode system. The "cavity transport coefficient" is defined.

2. Experimental Details

2.1. Chemical Reagents

Nitrobenzene, potassium ferrocyanide, nitrobenzene, and NaOH were obtained from Sigma-Aldrich UK. Chemical reagents were used as purchased, without further purification. Water was taken from a Thermo Scientific purification system (Barnstead Nanopure) with not less than 18.2 MOhm cm resistivity at 20 ^{o}C.

2.2. Instrumentation

Generator-collector experiments were performed on an Autolab PGSTAT30 bipotentiostat (Metrohm, UK) in four-electrode configuration with a platinum gauze and saturated calomel (SCE, Radiometer) as a counter and reference electrode respectively. Two types of dual working electrodes were used: (i) a gold-gold dual-plate working electrode, and (ii) a commercial gold-gold interdigitated array electrode (ED-IDA1-Au, Micrux Technologies, Spain). Gold-gold dual-plate microtrench electrodes were fabricated using a literature method [24] by cutting gold-coated microscope slides (Aldrich) into 1 cm × 3 cm strips using a diamond cutter (Buehler Isomet 1000 precision saw). The gold was then etched to leave a 5 mm strip down the middle of the slides and placed in a furnace at 500^{o}C for 30 minutes to oxidise the remaining titanium metal. Two gold slides were stuck together vis-à-vis using slow curing epoxy and cured at room temperature. Once cured, the end of the electrode was sliced off and polished flat and the epoxy was then etched for 5 minutes forming a microtrench between the two gold electrodes with dimensions of 5 mm length, 45 μm width (by SEM) and ca. 240 μm depth (estimated by voltammetry with the $Fe(CN)_6^{3-}$

$^{/4-}$ calibration redox system, see text). All experiments were conducted at a temperature of 22 ± 2 ^{o}C.

3. Theory

In order to define the dimensionless "cavity transport coefficient" $\Phi_{cavity} = \frac{flux\ due\ to\ inter-electrode\ diffusion}{flux\ due\ to\ external\ diffusion}$, the relative rate of mass transport needs to be expressed as a function of time for two components: for (i) the internal reversible redox cycle responsible for the generator-collector feedback current, and for (ii) the diffusion of bulk components to the dual-electrode followed by irreversible transformation.

For the dual-plate microtrench an approximate expression can be derived by dividing (i) the reversible Nernstian dual-plate diffusion current expression (ignoring time-dependent terms, equation 1) [25] by (ii) the diffusional current for a microband "inlet" (with time-dependent term, equation 2) [26,27] to give approximate equation 3 (see Figure 2).

$$I_{\text{internal}} = \frac{n_{\text{internal}} F D_{\text{internal}} l \times d \times c_{\text{internal}}}{\delta} \quad (1)$$

$$I_{\text{external}} = n_{\text{external}} F D_{\text{external}} l \times c_{\text{external}} \times \left[\frac{\pi e^{-2.5\sqrt{\frac{\pi D_{\text{external}} t}{\delta^2}}}}{4\sqrt{\frac{\pi D_{\text{external}} t}{\delta^2}}} + \frac{\pi}{\ln\left(\left[\frac{64 e^{-0.577} D_{\text{external}} t}{\delta^2} \right]^{1/2} + e^{5/3} \right)} \right] \quad (2)$$

$$\Phi_{microtrench} = \frac{I_{\text{internal}}}{I_{\text{external}}} = \frac{n_{\text{internal}}}{n_{\text{external}}} \times \frac{D_{\text{internal}}}{D_{\text{external}}} \times \frac{c_{\text{internal}}}{c_{\text{external}}} \times \frac{d}{\delta} \times \left[\frac{\pi e^{-2.5\sqrt{\frac{\pi D_{\text{external}} t}{\delta^2}}}}{4\sqrt{\frac{\pi D_{\text{external}} t}{\delta^2}}} + \frac{\pi}{\ln\left(\left[\frac{64 e^{-0.577} D_{\text{external}} t}{\delta^2}\right]^{1/2} + e^{5/3}\right)} \right]^{-1} \quad (3)$$

In these expressions n denotes the number of electrons transferred per molecule diffusing to the electrode, F is the Faraday constant, c is the concentration (with $c_{\text{internal}} = c_{ox} + c_{red}$ [17] to take into account the two components of the redox cycle), and the length l, the depth d, and the inter-electrode gap δ are geometric parameters. A plot of the cavity coefficient as a function of time t is shown in Figure 2C.

For the interdigitated microband array electrode system a similar approach can be employed to define the cavity transport coefficient Φ_{IDE} based on the steady state feedback current for the microband array (ignoring time-dependent terms and inserting band width = gap-width, equation 4 [1,28,29]) and the Cottrell equation (semi-infinite, time-dependent, see equation 5) ignoring edge terms.

$$I_{\text{internal}} = 0.49 \times N_{gap} \times n_{\text{internal}} F D_{\text{internal}} c_{\text{internal}} l \quad (4)$$

$$I_{\text{external}} = \frac{n_{\text{external}} F A_{IDE} \sqrt{D_{\text{external}}} c_{\text{external}}}{\sqrt{\pi}\sqrt{t}} \quad (5)$$

$$\Phi_{IDE} = \frac{I_{\text{internal}}}{I_{\text{external}}} = \frac{n_{\text{internal}}}{n_{\text{external}}} \times \frac{D_{\text{internal}}}{\sqrt{D_{\text{external}}}} \times \frac{c_{\text{internal}}}{c_{\text{external}}} \times \frac{0.49 \times N_{gap} \times l \times \sqrt{\pi}\sqrt{t}}{A_{IDE}} \quad (6)$$

Here, N_{gap} denotes the number of generator-collector gaps and A_{IDE} is the total active area over the interdigitated array. Both expressions for the cavity transport coefficient are time-dependent terms which have a characteristic effect over a timescale of

several seconds (see Figure 2C). Due to the strongly reduced diffusional access to the microtrench geometry, here the cavity transport coefficient is twice as high. This suggests that, at least to some extent, the generator-collector redox process is "decoupled" from the diffusion of reactive molecules from the bulk solution, which has implications for the chemical processes within the gap compared to those on the IDE. Also, the relative change in $\Phi_{microtrench}$ is much lower compared to that in Φ_{IDE}, which implies a more stable analytical signal.

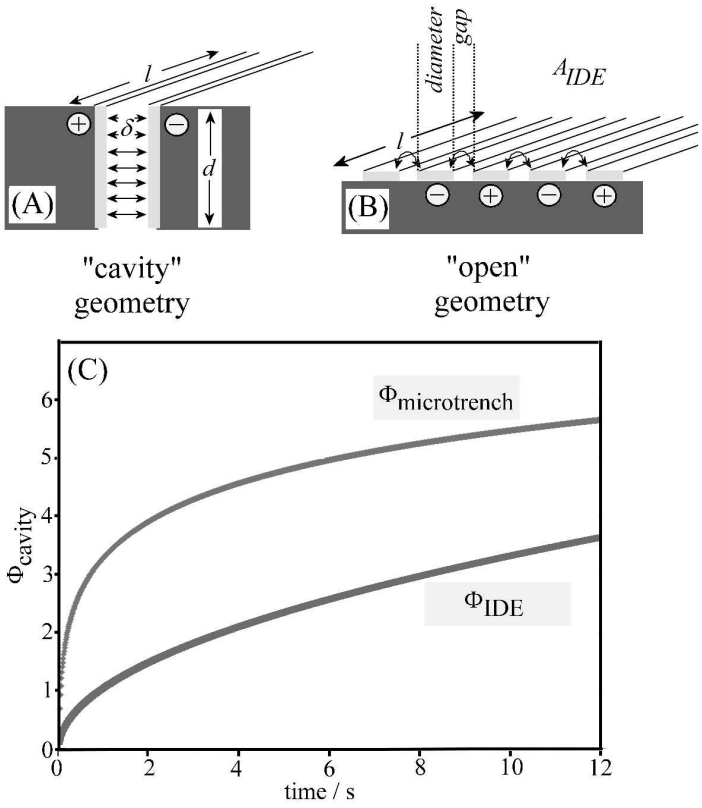

Figure 2. Schematic drawings for (A) the microtrench geometry and (B) the interdigitated electrode geometry with key parameters. (C) Plot of the cavity transport coefficient Φ_{cavity} for microtrench and for interdigitated array for $D = 0.6 \times 10^{-9}$ m^2s^{-1}, $n = 1$, $c_{internal} = c_{external}$ and geometric parameters as given above.

4. Results and Discussion

4.1. Au-Au Dual-Plate Generator-Collector Electrode: Ferrocyanide Calibration

In order to determine the depth of a dual-plate microtrench electrode a calibration redox system can be employed. Here the oxidation of ferrocyanide (equation 7) at the Au-Au dual-plate electrode is used (see Figure 3).

$$Fe(CN)_6^{4-}(aq) \rightleftharpoons Fe(CN)_6^{3-}(aq) + e^- \quad (7)$$

Figure 3A shows a typical cyclic voltammogram obtained at a 3 mm diameter gold disc electrode with a quasi-reversible oxidation and back-reduction centred at the reversible potential of 0.193 V vs. SCE. When investigated in an Au-Au dual-plate microtrench electrode (Figure 3B), the oxidation at the generator electrode is accompanied with the back-reduction of $Fe(CN)_6^{3-}$ at the collector electrode.

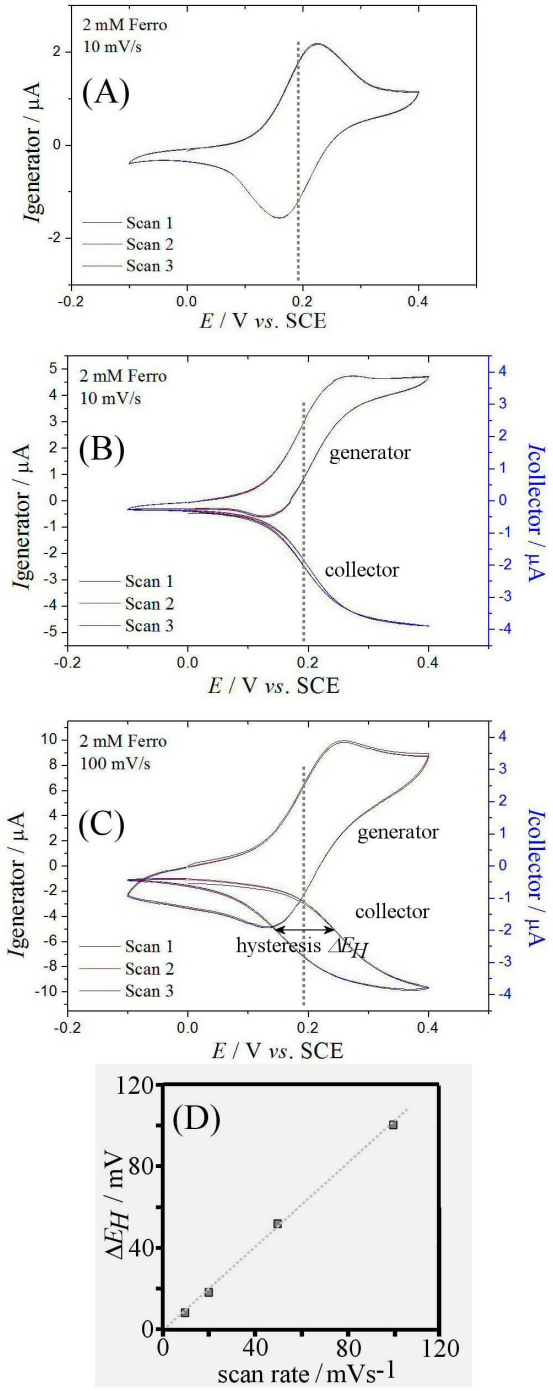

Figure 3. Cyclic voltammograms for the oxidation of 2 mM $Fe(CN)_6^{4-}$ in 0.1 M KCl (A) at a 1.6 mm diameter gold disc electrode (scan rate 10 mV s^{-1}) and (B) at a dual-plate Au-Au microtrench generator-collector electrode for the generator scanning and the collector fixed at -0.1 V vs. SCE (scan rate 10 mV s^{-1}), and (C) for the generator scanning and the collector potential fixed at -0.1 V vs. SCE (scan rate 100 mV s^{-1}). (D) Plot of the collector current hysteresis versus scan rate.

The generator current signal is associated with some capacitive charging and with some diffusion of reagent towards the microtrench. However, the collector current signal appears well-defined with a clear mass transport controlled limiting current. The magnitude of the collector limiting current, $I_{collector}$, for the dual-plate geometry can be written approximately as in equation 8 (compare equation 1).

$$I_{collector} = \frac{nFD_{Fe(CN)_6^{4-}} Ac_{Fe(CN)_6^{4-}}}{\delta} \quad (8)$$

In this equation n is the number of electrons transferred per molecule reacting at the electrode surface, F is the Faraday constant, $D_{Fe(CN)_6^{4-}}$ is the diffusion coefficient for $Fe(CN)_6^{4-}$ (additional effects from the slight difference in diffusion coefficients for $Fe(CN)_6^{4-}$ and $Fe(CN)_6^{3-}$ [17] are here assumed to be insignificant), A is the plate area, $c_{Fe(CN)_6^{4-}}$ is the bulk concentration of $Fe(CN)_6^{4-}$, and $\delta = 45$ μm is the inter-electrode gap. The hysteresis effect, ΔE_H, in the collector current (see Figure 3C) can be used to obtain an estimate for the diffusion coefficient (see equation 9 [30]).

$$D_{Fe(CN)_6^{4-}} = \frac{0.0071F\delta^2}{\Delta E_H RT} v \quad (9)$$

In this equation a linear trend is predicted for ΔE_H versus the scan rate v (see Figure 3D) and with the gas constant R and the absolute temperature T, the diffusion coefficient can be estimated as $D_{Fe(CN)_6^{4-}} = 0.6 \times 10^{-9}$ m^2s^{-1}. This value is in reasonable agreement with literature [31] and therefore employed throughout this study. Finally, the trench depth is obtained by rearranging equation 8 into equation 10.

$$\text{Trench depth} = \frac{I_{collector} \times \delta}{nFDwc} = 300\ \mu\text{m} \qquad (10)$$

In this equation w = 5 mm is the width of the microtrench and $I_{collector}$ is 3.6 μA (see Figure 3B). The average trench depth of 300 μm is consistent with an aspect ratio of between 6 to 7.

4.2. Au-Au Dual-Plate Generator-Collector Electrode: Reduction of Nitrobenzene

The reduction of nitrobenzene in alkaline media is known to follow a multi-step pathway [32,33] with an initial one-electron reduction to the unstable radical anion (see Figure 4A, P1, equation 11) followed by the transfer of another three electrons to give a mixture of products (see Figure 4A, P2).

$$NB(aq) + e^- \rightleftharpoons NB^{\cdot-}(aq) \qquad (11)$$

The one-electron process, P1, occurs at a midpoint potential of -0.7 V vs. SCE and is the focus of this study. When performed over a slightly wider potential window and at the Au-Au microtrench electrode (Figure 4B) a further sign of complexity is the presence of process P3, which is due to surface immobilised redox active products which further complicate the behaviour of the electrode (see Figure 4C). However, when working in generator – collector feedback mode, two well-defined collector processes are observed with a fixed collector potential at -0.2 V vs. SCE (Figure 4D).

The first minor reduction signal conssitent with process P3 is most likely due to oxygen reduction (all measurements were performed in the presence of ambient levels of dissolved oxygen). The second reduction signal is consistent with process P1 (see equation 11) and likely to be a one-electron feedback process.

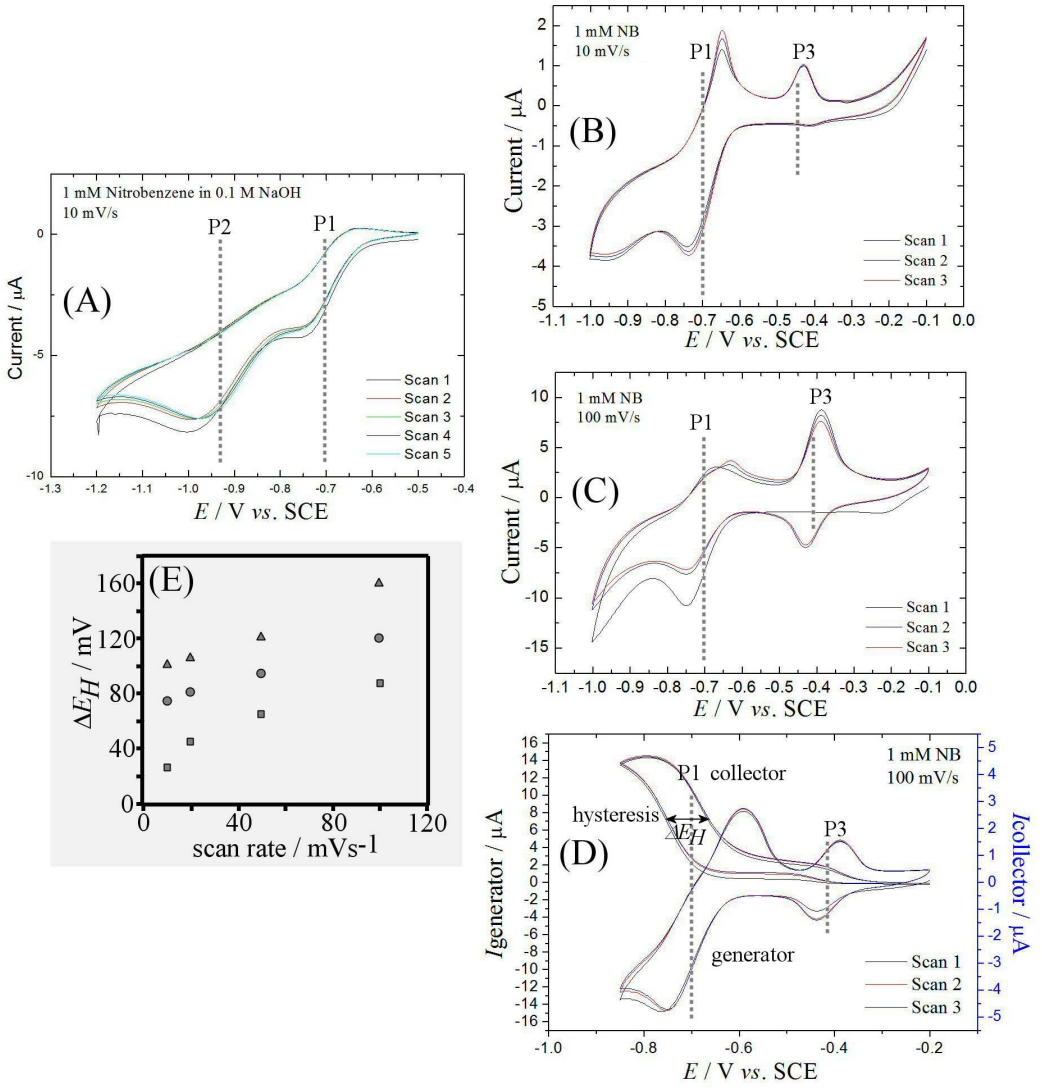

Figure 4. (A) Reduction of 1 mM nitrobenzene in 0.1 M NaOH (scan rate 10 mV s^{-1}) at a 3 mm diameter gold disc electrode. (B) Reduction of 1 mM nitrobenzene in 0.1 M NaOH (scan rate 10 mV s^{-1}) at Au-Au microtrench electrode with both electrodes scanning. (C) As before but with scan rate 100 mV s^{-1}. (D) Reduction of 1 mM nitrobenzene in 0.1 M NaOH at Au-Au microtrench with the generator electrode scanning and the collector potential fixed at -0.2 V vs. SCE. (E) Plot of the collector current hysteresis for the nitrobenzene reduction as a function of scan rate (square: 1 mM, circle: 0.1 mM, and triangle: 0.01 mM nitrobenzene concentration).

When analysing the mass transport limited collector current, $I_{collector}$ = ca. 3.3 μA, based on equation 8 and assuming a one-electron process, the nitrobenzene diffusion coefficient D_{NB} can be estimated (equation 12) in reasonable agreement (slightly high due to side reactions, *vide infra*) with literature values [34].

$$D_{NB} = \frac{I_{collector} \times \delta}{nFAc_{NB}} \approx 1.0 \times 10^{-9}\,\mathrm{m^2 s^{-1}} \qquad (12)$$

The hysteresis parameter ΔE_H, when plotted versus scan rate (Figure 4E), shows non-linear characteristics with non-zero intercept and concentration dependent values, probably due to the effects of deposited material and side reactions possibly with H_2O_2 produced during oxygen reduction. Further experiments were performed to investigate the low concentration feedback current for potential analytical applications. Figure 5 shows well-defined collector current responses for process P1 down to 1 μM nitrobenzene. Perhaps surprisingly, under conditions employed here in the presence of ambient levels of oxygen, the feedback current for the nitrobenzene oxidation at the collector electrode (potential fixed at -0.2 V vs. SCE) is substantially higher than that expected (see double logarithmic plot in Figure 5E). Also the generator current response is higher than expected (see line for linear behaviour). In order to explain this effect the presence of oxygen has to be taken into consideration as has been demonstrated recently for the reduction of $Ru(NH_3)_6^{3+}$ [35].

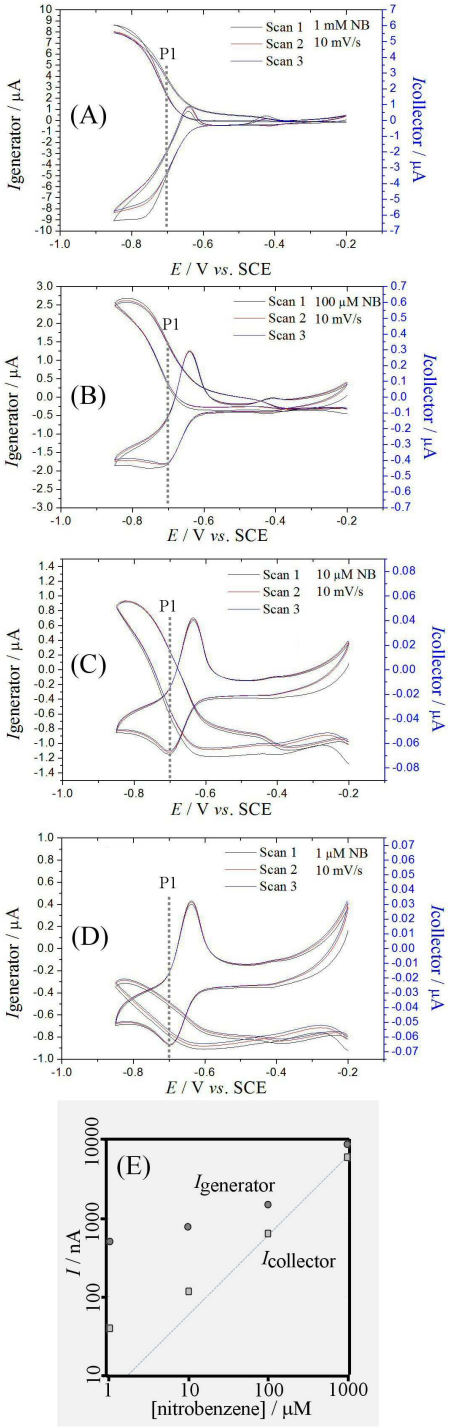

Figure 5. Cyclic voltammograms for the reduction of (A) 1 mM, (B) 0.1 mM, (C) 0.01 mM, (D) 0.001 mM nitrobenzene in 0.1 M NaOH (scan rate 10 mV s^{-1}) at Au-Au microtrench electrode with collector potential fixed at -0.2 V vs. SCE. (E) Double logarithmic plot of generator and collector current (mass transport controlled feedback currents) as a function of nitrobenzene concentration. Line indicates linear behaviour.

Compared to the generator current, the collector current signal is less sensitive to the presence of oxygen and could provide useful concentration data probably down to micromolar levels. In order to investigate the benefits of the Au-Au dual-plate microtrench electrode in this process, a comparison is now made to conventional interdigitated Au-Au band array electrodes.

4.3. Au-Au Interdigitated Array Generator-Collector Electrode: Oxidation of $Fe(CN)_6^{4-}$

Voltammetric current responses in generator – collector mode for the oxidation and re-reduction of 2 mM $Fe(CN)_6^{4-}$ in 0.1 M KCl are shown in Figure 6. Steady state limiting currents of several μA similar to those observed at the microtrench are detected with good collection efficiency.

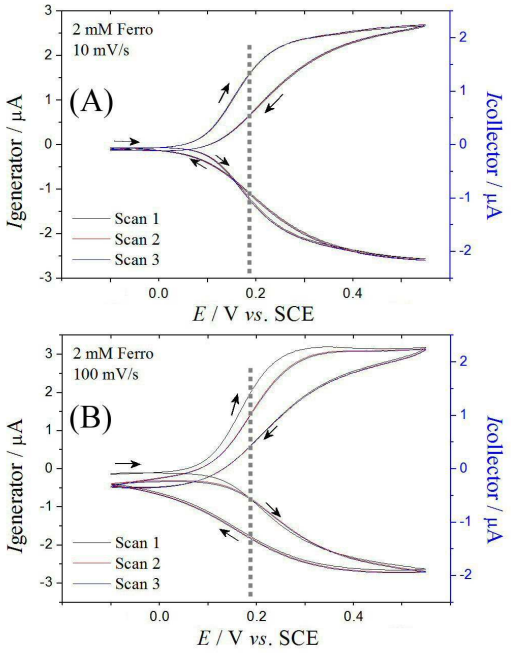

Figure 6. Cyclic voltammograms for the oxidation of 2 mM $Fe(CN)_6^{4-}$ in 0.1 M KCl (scan rate (A) 10 mV s^{-1} and (B) 100 mV s^{-1}) at an interdigitated array of Au band electrodes with collector potential -0.0 V vs. SCE.

The limiting currents at the generator and collector electrodes are almost independent of scan rate and determined here as 2.7 and negative 2.2 μA, respectively. This compares to the theoretically predicted collector current of 2.9 μA based on equation 4.

4.4. Au-Au Interdigitated Array Generator-Collector Electrode: Reduction of Nitrobenzene

When investigating the generator-collector current responses for the reduction of nitrobenzene in 0.1 M NaOH at the interdigitated array electrode, the process P1 at -0.7 V vs. SCE is clearly identified (Figure 7A). Both generator signal and collector signal are well-defined. However, when lowering the nitrobenzene concentration to 100 μM and 10 μM a drift in the collector signal is apparent. At a nitrobenezene concentration of 1 μM the generator current response is not observed anymore and the collector current response appears broadened. A double-logarithmic plot of collector current response versus nitrobenzene concentration (Figure 7E) shows a non-linear dependence more distorted compared to that for the microtrench electrode in Figure 5E. The reason for the non-linearity again is likely to be due to oxygen in the bulk solution and the increase in deviation from linearity here is likely to be linked to the lower cavity transport coefficient (see Figure 2C, oxygen can diffuse into the reaction zone at relatively higher rate).

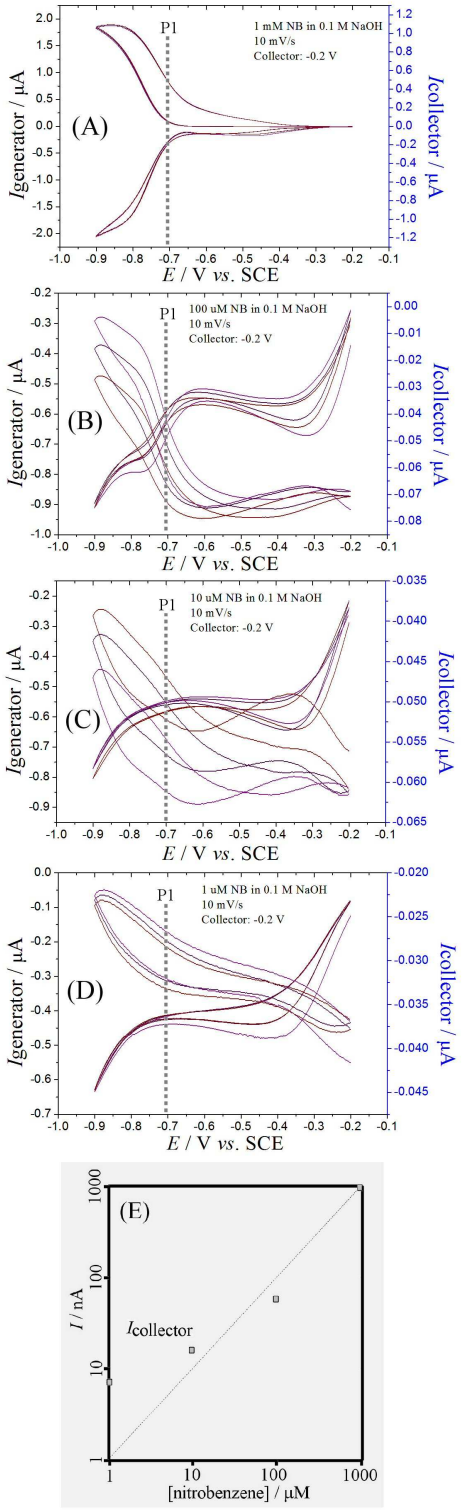

Figure 7. Cyclic voltammetry (scan rate 10 mV s^{-1}) for the reduction of (A) 1 mM, (B) 0.1 mM, and (C) 0.01 mM nitrobenzene in 0.1 M NaOH at an interdigitated Au band array electrode.

5. Summary and Conclusion

In a comparison of (i) a dual-plate microtrench electrode and (ii) an interdigitated array electrode similarities and differences in electroanalytical performance have been investigated. Both types of electrodes gave very similar voltammetric responses for the oxidation of $Fe(CN)_6^{4-}$ confirming theoretical prediction. However, when investigated under less ideal conditions employing a more complex nitrobenezene redox system and aerated solution, the interdigitated array electrode exhibits more drift in signals and less tolerance towards oxygen. The "cavity transport coefficient" Φ_{cavity} was introduced to quantify the relative rates of diffusion within the redox cycle feedback and from outside bulk solution. The dual-plate microtrench electrode has a more stable and higher Φ_{cavity}, which is readily increased further by etching deeper into the trench.

For a more quantitative treatment of the diffusion-reaction chemistry within the generator-collector electrode system, computational simulation tools addressing the electrode geometry and the distribution of chemical intermediates will have to be developed in future. This will be particularly helpful in unravelling the feedback current enhancing effect of dioxygen. Benefits of the dual-plate microtrench electrode can be summarised as (i) more stable current responses, (ii) less interference form reagents (e.g. oxygen) diffusing in from the bulk, and (iii) less sensitivity to convection in the bulk. Both sensitivity and Φ_{cavity} are readily improved by varying the geometric parameters. In future, dual-plate microtrench electrodes could be manufactured in a range of sizes down to nanotrench level and they will provide a novel and powerful electroanalytical tool.

Acknowledgements

S.E.C.D. and F.M. thank EPSRC (EP/I028706/1) and G.E.M.L. thanks NERC for funding.

References

[1] E.O. Barnes, G.E.M. Lewis, S.E.C. Dale, F. Marken and R.G. Compton, *Analyst*, 2012, **137**, 1068.

[2] A. Rene, C. Cugnet, D. Hauchard and L. Authier, *Analyst*, 2013, **138**, 2192.

[3] A. Aggarwal, M.J. Hu and I. Fritsch, *Anal. Bioanal. Chem.*, 2013, **405**, 3859.

[4] A. Oleinick, F. Zhu, J.W. Yan, B.W. Mao, I. Svir and C. Amatore, *ChemPhysChem*, 2013, **14**, 1887.

[5] K.C. Honeychurch, G.C. Smith and J.P. Hart, *Anal. Chem.*, 2006, **78**, 416.

[6] A.C. Fisher, R.G. Compton, C.M.A. Brett and A.M.C.F.O. Brett, *J. Electroanal. Chem.*, 1991, **318**, 53.

[7] G.E.M. Lewis, S.E.C. Dale, B. Kasprzyk-Hordern, E.O. Barnes, R.G. Compton and F. Marken, *Electroanalysis*, 2012, **24**, 1726.

[8] Y. Luo, C. Liu, Y.Y. Qu and N. Fang, *Bioanalysis*, 2012, **4**, 453.

[9] K. Aoki, K. Tokuda and H. Matsuda, *J. Electroanal. Chem.*, 1985, **195**, 229.

[10] C. Amatore, N. Da Mota, C. Lemmer, C. Pebay, C. Sella and L. Thouin, *Anal. Chem.*, 2008, **80**, 9483.

[11] H. Rajantie, J. Strutwolf and D.E. Williams, *J. Electroanal. Chem*., 2001, **500**, 108.

[12] I. Streeter, N. Fietkau, J. Del Campo, R. Mas, F.X. Munoz and R.G. Compton, *J. Phys. Chem. C*, 2007, **111**, 12058.

[13] L. Rassaei, P.S. Singh and S.G. Lemay, *Anal. Chem*., 2011, **83**, 3974.

[14] I.J. Cutress and R.G. Compton, *J. Electroanal. Chem.*, 2010, **645**, 159.

[15] S.E.C. Dale, Y.H. Chan, P.C.B. Page, E.O. Barnes, R.G. Compton and F. Marken, *Electrophoresis*, 2013, **34**, 1979.

[16] J.L. Hammond, A.J. Gross, P. Estrela, J. Iniesta, S.J. Green, C.P. Winlove, P.G. Winyard, N. Benjamin and F. Marken, *Anal. Chem*., 2014, DOI: 10.1021/ac501321e.

[17] S.E.C. Dale, A. Vuorema, M. Sillanpää, J. Weber, A.J. Wain, E.O. Barnes, R.G. Compton and F. Marken, *Electrochim. Acta*, 2014, **125**, 94.

[18] A.J. Gross and F. Marken, *Electrochem. Commun.*, 2014, DOI: 10.1016/j.elecom.2014.06.025.

[19] M.A. Hasnat, A.J. Gross, S.E.C. Dale, E.O. Barnes, R.G. Compton and F. Marken, *Analyst*, 2014, **139**, 569.

[20] C.K. Chua and M. Pumera, *Electroanalysis*, 2011, **23**, 2350.

[21] X. Ceto, A.M. O' Mahony, J. Wang and M. del Valle, *Talanta*, 2013, **107**, 270.

[22] F. Marken, S. Kumbhat, G.H.W. Sanders and R.G. Compton, *J. Electroanal. Chem*., 1996, **414**, 95.

[23] B. Kastening and S. Vavricka, *Ber. Bunsen-Gesell. Phys. Chem.*, 1968, **72**, 27.

[24] S.E.C. Dale and F. Marken, *Faraday Disc.*, 2013, **164**, 349.

[25] R.G. Compton and C.E. Banks, *Understanding Voltammetry*, World Scientific, London, 2007, 95.

[26] A. Szabo, D.K. Cope, D.E. Tallman, P.M. Kovach and R.M. Wightman, *J. Electroanal. Chem.*, 1987, **217**, 417.

[27] C. Amatore in I. Rubinstein, *Physical Electrochemistry*, Marcel Dekker, New York, 1995, 155.

[28] K. Aoki, M. Morita, O. Niwa and H. Tabei, *J. Electroanal. Chem.*, 1988, **256**, 269.

[29] K. Aoki and M. Tanaka, *J. Electroanal. Chem.*, 1989, **266**, 11.

[30] A. Vuorema, H. Meadows, N. Bin Ibrahim, J. Del Campo, M. Cortina-Puig, M.Y. Vagin, A.A. Karyakin, M. Sillanpää and F. Marken, *Electroanalysis*, 2010, **22**, 2889.

[31] R.N. Adams, *Electrochemistry at Solid Electrodes*, Marcel Dekker, New York, 1969, 220.

[32] I. Rubinstein, *J. Electroanal. Chem.*, 1985, **183**, 379.

[33] P. Zuman, Z. Fijalek, D. Dumanovic and D. Suznjevic, *Electroanalysis*, 1992, **4**, 783.

[34] J. Marquez and D. Pletcher, *J. Appl. Electrochem.*, 1980, **10**, 567.

[35] S.E.C. Dale, C.E. Hotchen and F. Marken, *Electrochim. Acta*, 2013, **101**, 196.